

Tuning of the $[\text{Cu}_3(\mu\text{-O})]^{4+/5+}$ Redox Couple: Spectroscopic Evidence of Charge Delocalization in the Mixed-Valent $[\text{Cu}_3(\mu\text{-O})]^{5+}$ Species

Marlyn Rivera-Carrillo,[†] Indranil Chakraborty,[†] Gellert Mezei,^{†,‡} Richard D. Webster,[§] and Raphael G. Raptis^{*,†}

Department of Chemistry, University of Puerto Rico, P.O. Box 23346, San Juan, Puerto Rico 00931-3346, and Division of Chemistry and Biological Chemistry, School of Physical and Mathematical Sciences, Nanyang Technological University, Singapore 637371

Received March 24, 2008

Trinuclear Cu^{II} -complexes of formula $[\text{Cu}^{\text{II}}_3(\mu_3\text{-E})(\mu\text{-4-R-pz})_3\text{X}_3]^{\pm n}$, E = O and OH; R = H, Cl, Br, CH(O) and NO_2 ; X = Cl, NCS, CH_3COO , and py, have been synthesized and characterized and the effect of substitution of terminal ligands, as well as 4-R-groups, in the one-electron oxidation process has been investigated by cyclic voltammetry. In situ UV–vis–NIR spectroelectrochemical characterization of the mixed valence Cu_3^{7+} -complex $[\text{Cu}_3(\mu_3\text{-O})(\mu\text{-pz})_3\text{Cl}_3]^-$ revealed an intervalence charge transfer band at 9550 cm^{-1} ($\epsilon = 2600\text{ cm}^{-1}\text{ M}^{-1}$), whose analysis identifies this species as a delocalized, Robin–Day class-III system, with an electronic coupling factor, H_{ab} , of 4775 cm^{-1} .

Introduction

Redox-active trinuclear copper clusters catalyze the four-electron reduction of dioxygen to water in the active centers of multicopper blue oxidase, such as ascorbate oxidases, laccase, and ceruloplasmin.¹ Four Cu-centers cycling between +1 and +2 oxidation states or a single trinuclear unit cycling between Cu_3^{3+} and a mixed-valent Cu_3^{7+} state may participate in the reduction process. Particulate Methane Monooxygenase (pMMO), a membrane protein of methanotrophic bacteria responsible for the regioselective oxidation of $\text{C}_1\text{--C}_5$ alkanes to their corresponding alcohols, has also been proposed by Chan et al. to employ multiple tricopper clusters in its active center.² This claim has been contradicted by spectroscopic data,³ as well as by an X-ray crystallographic

study of an, alas, catalytically inert pMMO sample, showing only one dinuclear and one remote mononuclear Cu-sites.⁴ In two recent articles, however, Chan et al. have restated the multitrinuclear Cu-cluster hypothesis based on new EPR spectroscopic evidence.⁵ Furthermore, the new studies, employing a synthetic, catalytically active Cu_3 -model system, have identified a triangular, formally $\text{Cu}^{\text{II}}_2\text{Cu}^{\text{III}}(\mu_3\text{-O})$ intermediate as the O-transfer species.^{5b}

Structural, as well as spectroscopic data on triangular $\text{Cu}^{\text{II/III}}$ systems that might model the latter intermediate are scarce. A bis-capped $\text{Cu}_3(\mu_3\text{-O})_2^{5+}$ species has been shown by crystallographic and spectroscopic analyses to contain distinct Cu^{III} and ferromagnetically coupled Cu^{II} sites, a valence-trapped complex ($^3\text{A}_2$ ground state).⁶ The latter system has also been analyzed by density functional theory (DFT) calculations.⁷ In contrast, a structurally related $\text{Cu}_3(\mu_3\text{-S})_2^{5+}$ complex has been shown to be valence-delocalized (^3E ground state).⁸ We have reported the one-electron electrochemical oxidation of $[\text{Cu}^{\text{II}}_3(\mu_3\text{-O})(\mu\text{-pz})_3\text{X}_3]^{2-}$, pz = pyrazolate anion, $\text{C}_3\text{H}_3\text{N}_2^-$, X = Cl (1^{2-}), CF_3COO (2^{2-}), and

* To whom correspondence should be addressed. E-mail: raphael@adam.uprr.pr.

[†] University of Puerto Rico.

[‡] Current address: Department of Chemistry, College of Arts and Sciences, 3425 Wood Hall, Western Michigan University, Kalamazoo, MI 49008-3842.

[§] Nanyang Technological University.

- (1) (a) Gatteschi, D.; Caneschi, A.; Pardi, L.; Sessoli, R. *Science* **1994**, *265*, 1054. (b) Gatteschi, D.; Sessoli, R. *Angew. Chem.* **2003**, *42*, 268.
- (2) (a) Nguyen, H.-H. T.; Shiemke, A. K.; Jacobs, S. J.; Hales, B. J.; Lidstrom, M. E.; Chan, S. I. *J. Biol. Chem.* **1994**, *269*, 14995. (b) Wilkinson, B.; Zhu, M.; Priestley, N. D.; Nguyen, H. H. T.; Morimoto, H.; Williams, P. G.; Chan, S. I.; Floss, H. G. *J. Am. Chem. Soc.* **1996**, *118*, 921. (c) Elliot, S. J.; Zhu, M.; Tso, L.; Nguyen, H. H. T.; Yip, J. H.-K.; Chan, M. K. *J. Am. Chem. Soc.* **1997**, *119*, 9949. (d) Chan, S. I. *J. Inorg. Biochem.* **1999**, *74*, 17.

- (3) Yuan, H.; Collins, J. P.; Antholine, W. E. *J. Am. Chem. Soc.* **1997**, *119*, 5073.

- (4) Lieberman, R. L.; Rosenzweig, A. C. *Nature* **2005**, *434*, 177.

- (5) (a) Chan, S. I.; Wang, V. C. C.; Lai, J. C. H.; Yu, S. S. F.; Chen, P. P. Y.; Chen, K. H. C.; Chen, C. L.; Chan, M. K. *Angew. Chem., Int. Ed.* **2007**, *46*, 1992. (b) Chen, P. P.-Y.; Yang, R. B.-G.; Lee, J. C.-M.; Chan, S. I. *Proc. Natl. Acad. Sci. U.S.A.* **2007**, *104*, 14571.

- (6) Cole, A. P.; Root, D. E.; Mukherjee, P.; Solomon, E. I.; Stack, T. D. P. *Science* **1996**, *120*, 1848.

the structural characterization of the oxidized, mixed-valent species 3^- ($X = \text{O}_2\text{CPh}$).⁹ A theoretical analysis by DFT calculations of the latter has shown it to be a valence-delocalized Cu_3^{7+} species ($^1\text{A}_1$ ground state).⁹ Belinsky has interpreted the different electronic structures of the above three Cu_3^{7+} systems in terms of the relationship between the energy levels and the double-exchange parameter values H_{ab} , estimating an H_{ab} value of approximately 5000 cm^{-1} for 3^- .¹⁰ Complex 3^- is the only known, albeit not fully studied, structural and valence analogue of the fully oxidized pMMO state proposed by Chan et al.^{5b} In further pursuit of such models, in this article we follow up on our earlier work on tricopper pyrazolates of formula $[\text{Cu}^{\text{II}}_3(\mu_3\text{-O})(\mu\text{-4-R-pz})_3\text{X}_3]^{2-}$ by studying the influence of substitution of terminal ligands-X and 4-R-groups on the electrochemical potential of the $\text{Cu}^{\text{II}}_3(\mu_3\text{-O})^{4+/5+}$ redox couple.^{9,11} Herein, we present the synthesis and characterization of new trinuclear complexes $(\text{PPN})_3[\text{Cu}^{\text{II}}_3(\mu_3\text{-O})(\mu\text{-4-R-pz})_3\text{X}_3]\text{Cl}$, $X = \text{Cl}$, $R = \text{Br}$ (**4**), Cl (**5**), CHO (**6**), and NO_2 (**7**), $(\text{Bu}_4\text{N})[\text{Cu}^{\text{II}}_3(\mu_3\text{-OH})(\mu\text{-4-R-pz})_3\text{X}_3]$, $R = \text{H}$, $X = \text{NCS}$ (**8**), and $[\text{Cu}^{\text{II}}_3(\mu_3\text{-OH})(\mu\text{-4-R-pz})_3\text{X}_3](\text{CF}_3\text{CO}_2)_2$, $R = \text{H}$, $X = \text{py}$ (**9**). In addition, we present the electrochemical studies of the $(\mu_3\text{-O})$ complexes **4–7** and the corresponding species resulting from the in situ deprotonation of the $(\mu_3\text{-OH})$ complexes **8, 9**, and **10** ($R = \text{H}$, $X = \text{CH}_3\text{CO}_2$). We also present the in situ UV–vis–NIR spectroelectrochemical characterization of the mixed-valent $[\text{Cu}_3(\mu_3\text{-O})(\mu\text{-pz})_3\text{X}_3]^-$ (**1**⁻).

Experimental Section

Materials and Methods. All commercially available reagents were used as received. Solvents were purified using standard techniques.¹² Literature procedures were followed for the synthesis of 4-Cl-pzH,¹³ 4-Br-pzH,¹³ 4-NO₂-pzH,¹⁴ 4-CHO-pzH,¹⁵ $(\text{PPN})_2[\text{Cu}_3(\mu_3\text{-O})(\mu\text{-pz})_3\text{Cl}_3]$ (**1**),^{11a} and $(\text{PPN})[\text{Cu}_3(\mu_3\text{-OH})(\mu\text{-pz})_3(\text{O}_2\text{CCH}_3)_3(\text{H}_2\text{O})] \cdot (\text{H}_2\text{O})$ (**10**).¹⁶

Physical Measurements. Elemental analyses were performed by Galbraith Laboratories, Inc., Knoxville, TN. Infrared, NMR and UV–vis spectra were recorded at room temperature on a Bruker Tensor 27, Bruker Avance DPX-300/DRX-500 and Varian Cary 500 Scan, respectively. Electrochemical measurements were performed on a BAS CV-50W voltammetric analyzer with Pt working

and auxiliary electrodes, Ag/AgNO₃ reference electrode, and 0.5 M in $\text{Bu}_4\text{NPF}_6/\text{CH}_2\text{Cl}_2$ as electrolyte. All potentials are reported relative to the ferrocene/ferrocenium reference couple. This was accomplished by adding ferrocene as an internal standard after recording the voltammetry of each analyte. Melting points were measured on an Electrothermal IA9100 apparatus and reported without correction. The in situ spectroelectrochemical experiment was carried out on a Varian Cary 5E UV–vis–NIR spectrophotometer equipped with an Optically Semitransparent Thin Layer Electrode (OSTLE) cell.¹⁷

X-ray diffraction data were collected with a Bruker AXS SMART 1K CCD diffractometer,¹⁸ using graphite-monochromated Mo K α radiation at ambient temperature from single crystals mounted atop glass fibers at a random orientation. Data were corrected for Lorentz and polarization effects.¹⁹ The structures were solved employing the SHELXTL-direct methods program and refined by full-matrix least-squares on F^2 .²⁰ Crystallographic details are summarized in Table 1.

(PPN)₃[Cu₃(μ_3 -O)(μ -4-Br-pz)₃Cl₃]Cl (4**). Method A.** $\text{CuCl}_2 \cdot 2\text{H}_2\text{O}$ (511 mg, 3.00 mmol), 4-bromo-pyrazole (441 mg, 3.00 mmol), NaOH (120 mg, 3.00 mmol), and PPNCl (1.722 g, 3.00 mmol) were stirred in 25 mL of CH_2Cl_2 for 1 day, at ambient temperature. After filtration, the green solution was evaporated to one-half. Addition of 50 mL of Et_2O precipitated out a green solid, which was filtered out, washed with Et_2O , air-dried, and recrystallized from $\text{CH}_2\text{Cl}_2/\text{DME}$ as dark green crystals to obtain $(\text{PPN})_3[\text{Cu}_3(\mu_3\text{-Cl})_2(\mu\text{-Br-pz})_3\text{Cl}_3]\text{Cl} \cdot 3\text{H}_2\text{O}$ (2.158 g, 85.9%). Anal. Calcd/Found: C, 55.96/55.61; H, 4.10/3.91; N, 5.02/5.10. $(\text{PPN})_3[\text{Cu}_3(\mu_3\text{-Cl})_2(\mu\text{-Br-pz})_3\text{Cl}_3]\text{Cl} \cdot 3\text{H}_2\text{O}$ (75.3 mg, 0.03 mmol) was dissolved in 2 mL of CH_2Cl_2 , and 0.2 mL of methanolic solution containing NaOH (4.8 mg, 0.12 mmol) were added under stirring. The green color of the solution immediately turned darker. After 5 h the solution was filtered, and Et_2O was allowed to slowly diffuse into the filtrate yielding 56.3 mg (78%) of crystalline product.

Method B. Complex **4** was prepared similarly as **1**^{11a} using 6 equiv of NaOH, $\text{CuCl}_2 \cdot 2\text{H}_2\text{O}$ (140.6 mg, 0.82 mmol), 4-Br-pzH (123.4 mg, 0.84 mmol), NaOH (68.5 mg, 1.71 mmol), and PPNCl (477.3 mg, 0.80 mmol). The reaction mixture was stirred overnight, and then it was filtered and set up for $\text{Et}_2\text{O}/\text{CH}_2\text{Cl}_2$ diffusion. Violet crystals were manually separated from a mixture of green, blue, and violet crystals and then were washed with chilled acetone and THF, dissolved, and crystallized twice from $\text{Et}_2\text{O}/\text{CH}_2\text{Cl}_2$. Yield: 135.2 mg (21.1%) of crystalline **4**. Anal. Calcd/Found: C, 57.64/57.11; H, 4.13/3.69; N, 5.17/5.34. Mp. (239.8–240.1) °C. UV–vis (CH_2Cl_2 , cm^{-1}): 14771, 25840 (sh), 29940 (sh), 36496 (sh), 37313, 38168 (sh). IR (cm^{-1}): 3673 (vw), 3561 (vw), 3049 (vw), 1587 (w), 1481 (w), 1436 (m), 1387 (w), 1297 (sh), 1283 (sh), 1266 (s), 1180 (w), 1152 (w), 1113 (s), 1049 (m), 1027 (w), 995 (m), 951 (m), 836 (m), 803 (w), 765 (w), 746 (m), 722 (s), 689 (s), 610 (m), 549 (s), 534 (s), 526 (sh), 495 (s), 440 (w).

(PPN)₃[Cu₃(μ_3 -O)(μ -4-Cl-pz)₃Cl₃]Cl (5**). Method A.** Complex **5** was prepared similarly as **4**, using 4-Cl-pzH to obtain $(\text{PPN})_3[\text{Cu}_3(\mu_3\text{-Cl})_2(\mu\text{-Cl-pz})_3\text{Cl}_3]\text{Cl} \cdot 3\text{H}_2\text{O}$. Anal. Calcd/Found: C, 60.47/60.18; H, 4.17/4.22; N, 5.43/5.63; Cl, 13.73/14.74. Further reaction with a methanolic solution containing NaOH and crystallization from Et_2O diffusion afforded crystalline **5** in 78%.

Method B. Complex **5** was prepared similarly as **4** using $\text{CuCl}_2 \cdot 2\text{H}_2\text{O}$ (141.5 mg, 0.82 mmol), 4-Cl-pzH (85.6 mg, 0.84

- (7) (a) Bérces, A. *Chem.—Eur. J.* **1998**, *4*, 1297. (b) Root, D. E.; Henson, M. J.; Machonkin, T.; Mukherjee, P.; Stack, T. D. P.; Solomon, E. I. *J. Am. Chem. Soc.* **1998**, *120*, 4982. (c) Daul, C.; Fernandez-Ceballos, S.; Ciofini, I.; Rauzy, C.; Schlöpfer, C.-W. *Chem.—Eur. J.* **2002**, *8*, 4392.
 (8) Brown, E. C.; York, J. T.; Antholine, W. E.; Ruiz, E.; Alvarez, S.; Tolman, W. B. *J. Am. Chem. Soc.* **2005**, *127*, 13752.
 (9) Mezei, G.; McGrady, J. E.; Raptis, R. G. *Inorg. Chem.* **2005**, *44*, 7271.
 (10) Belinski, M. I. *Inorg. Chem.* **2006**, *45*, 9096.
 (11) (a) Angaridis, P. A.; Baran, P.; Boca, R.; Cervantes-Lee, F.; Haase, W.; Mezei, G.; Raptis, R. G.; Werner, R. *Inorg. Chem.* **2002**, *41*, 2219. (b) Boca, R.; Dhlán, L.; Mezei, G.; Ortiz-Pérez, T.; Raptis, R. G.; Telsler, J. *Inorg. Chem.* **2003**, *42*, 5801. (c) Mezei, M.; Raptis, R. G.; Telsler, J. *Inorg. Chem.* **2006**, *45*, 8841.
 (12) Perrin, D. D. In *Purification of Laboratory Chemicals*; Perrin, D. D.; Armarego, W. L. F.; Perrin D. R., Eds.; Pergamon Press: Oxford, 1980.
 (13) Ehler, M. K.; Rettig, S. J.; Storr, A.; Thompson, R. C.; Trotter, J. *Can. J. Chem.* **1991**, *69*, 432.
 (14) Maresca, K. P.; Rose, D. J.; Zubieta, J. *Inorg. Chim. Acta* **1997**, *260*, 83.
 (15) Takagi, K.; Bajnati, A.; Hubert-Habart, M. *Bull. Soc. Chim. Fr.* **1990**, *127*, 660.
 (16) Mezei, G.; Rivera-Carrillo, M.; Raptis, R. G. *Inorg. Chim. Acta* **2004**, *357*, 3721.

- (17) Duff, C. M.; Heath, G. A. *Inorg. Chem.* **1991**, *30*, 2528.
 (18) *Data Collection: SMART-NT Software Reference Manual*, version 5.0; Bruker AXS, Inc.: Madison, WI, 1998.
 (19) *Data Reduction: SAINT-NT Software Reference Manual*, version 4.0; Bruker AXS, Inc.: Madison, WI, 1996.
 (20) Sheldrick, G. M. *Acta Crystallogr.* **2008**, *A64*, 112.

Table 1. Crystallographic Data and Structure Refinement for 4–9

	4·H ₂ O	5·H ₂ O	6·H ₂ O	7	8	9·(CH ₃) ₂ CO
empirical formula	C ₁₁₇ H ₉₈ Br ₃ Cl ₄ Cu ₃ N ₉ O ₂ P ₆	C ₁₁₇ H ₉₈ Cl ₇ Cu ₃ N ₉ O ₂ P ₆	C ₁₂₀ H ₁₀₁ Cl ₄ Cu ₃ N ₉ O ₅ P ₆	C ₁₁₇ H ₉₆ Cl ₄ Cu ₃ N ₁₂ O ₇ P ₆	C ₂₈ H ₄₆ Cu ₃ N ₁₀ OS ₃	C ₂₉ H ₃₁ Cu ₃ F ₆ O ₈ S ₂
<i>f</i> _w	2420.01	2286.63	2267.34	2300.30	825.55	1002.37
temp (K)	298(2)	298(2)	298(2)	298(2)	298(2)	298(2)
wavelength (Å)	0.71073	0.71073	0.71073	0.71073	0.71073	0.71073
cryst syst	trigonal	trigonal	trigonal	trigonal	trigonal	monoclinic
space group	R3	R3	R3	R3	R3	P2(1)/c
<i>a</i> (Å)	22.857(2)	22.840(2)	22.908(3)	22.944(2)	8.5880(15)	14.473(3)
<i>b</i> (Å)	22.857(2)	22.840(2)	22.908(3)	22.944(2)	12.385(2)	11.203(2)
<i>c</i> (Å)	18.075(2)	17.956(2)	17.874(5)	17.826(3)	18.017(3)	25.081(5)
α (deg)	90	90	90	90	90	90
β (deg)	90	90	90	90	97.561(3)	93.013(4)
γ (deg)	120	120	120	120	96.662(3)	90
volume (Å ³)	8178(1)	8112(1)	8123(3)	8127(2)	1862.9(6)	4061(1)
<i>Z</i>	3	3	3	3	2	4
density (calcd.) (Mg m ⁻³)	1.474	1.404	1.390	1.410	1.472	1.639
abs coeff (mm ⁻¹)	1.921	0.902	0.831	0.834	1.902	1.744
Flack parameter	−0.029(9)	0.053(15)	−0.042(12)	0.08(3)		
<i>F</i> (000)	3687	3525	3507	3549	854	2020
cryst size (mm)	0.20 × 0.20 × 0.13	0.18 × 0.12 × 0.10	0.40 × 0.27 × 0.15	0.11 × 0.10 × 0.09	0.18 × 0.14 × 0.10	0.18 × 0.16 × 0.12
no. of independent refls	12097	11980	12964	14319	9127	20697
<i>R</i>	0.0292	0.0383	0.0338	0.0572	0.0477	0.0552
<i>R</i> _w	0.0361	0.0582	0.0367	0.1191	0.1087	0.1346

mmol), NaOH (68.7 mg, 1.71 mmol), and PPNCI (496.5 mg, 0.84 mmol). Yield: 129.0 mg of crystalline **5** (20.8%). Anal. Calcd/Found: C, 60.97/60.80; H, 4.37/4.18; N, 5.47/5.58. Mp. (226.7–228.0) °C. ¹H NMR (CD₂Cl₂, ppm): 22.40 (6H, *w*_{1/2} = 550 Hz). IR (cm⁻¹): 3673 (vw), 3560 (vw), 3051 (vw), 2695 (vw), 1587 (w), 1506 (vw), 1481 (w), 1435 (m), 1392 (w), 1370 (vw), 1264 (s), 1209 (w), 1180 (w), 1164 (w), 1150 (w), 1113 (s), 1050 (m), 1026 (w), 994 (m), 964 (m), 834 (m), 804 (w), 763 (w), 748 (m), 722 (s), 688 (s), 614 (m), 549 (s), 533 (s), 495 (s), 460 (vw), 449 (vw), 438 (vw). UV–vis (CH₂Cl₂, cm⁻¹): 14771, 26110 (sh), 29940 (sh), 36496 (sh), 37313, 38168 (sh).

(PPN)₃[Cu₃(μ₃-O)(μ-4-CHO-pz)₃Cl₃]Cl (**6**). CuCl₂·H₂O (141.3 mg, 0.83 mmol), 4-CHO-pzH (79.6 mg, 0.83 mmol), NaOH (66.2 mg, 1.66 mmol), and PPNCI (481.9 mg, 0.81 mmol) were added to 10 mL of CH₂Cl₂ under stirring. 4-CHO-pzH was dissolved in 2 mL of ethyl acetate prior to addition. The reaction mixture was stirred overnight, was filtered, and the product was precipitated with 100 mL of Et₂O. The solid obtained (308.6 mg) was washed with THF and chilled CH₂Cl₂. Then, the product was crystallized by slow Et₂O vapor diffusion into a CH₂Cl₂ solution of **6**. Violet crystals (147.8 mg, 24.5%) were manually separated under a microscope. Anal. Calcd/Found: C, 63.06/62.83; H, 4.54/4.49; N, 5.52/5.58. Mp. (196.9–198.8) °C. ¹H NMR (CD₂Cl₂, ppm): 25.35 (6H, *w*_{1/2} = 750 Hz); 16.87 (3H, *w*_{1/2} = 500 Hz). IR (cm⁻¹): 3051 (w), 2763 (w), 2704 (w), 1676 (s), 1587 (w), 1530 (m), 1481 (w), 1435 (m), 1416 (w), 1264 (s), 1207(m), 1112 (s), 1056 (m), 1010 (m), 996 (m), 872 (w), 803 (w), 765 (w), 721 (s), 689 (s), 626 (m), 549 (s), 533 (s), 496 (s), 460 (vw), 449 (vw), 438 (vw). UV–vis (CH₂Cl₂, cm⁻¹): 14771, 26178, 36364 (sh), 37736 (sh), 38462 (sh), 39370 (sh).

(PPN)₃[Cu₃(μ₃-O)(μ-4-NO₂-pz)₃Cl₃]Cl (**7**). CuCl₂·H₂O (141.2 mg, 0.82 mmol), 4-NO₂-pzH (93.4 mg, 0.83 mmol), NaOH (68.7 mg, 1.72 mmol), and PPNCI (473.4 mg, 0.80 mmol) were added to 10 mL of CH₂Cl₂ under stirring. 4-NO₂-pzH was dissolved in 2 mL of methanol prior to addition. The reaction mixture was stirred overnight, was filtered, and the product was precipitated with Et₂O. The solid obtained (200.4 mg) was washed with THF and chilled acetone. Then, the product was crystallized by slow Et₂O vapor diffusion into the CH₂Cl₂ solution of **7**. Violet crystals (80.2 mg, 13.1%) were manually separated under a microscope. Anal. Calcd/Found: C, 60.15/59.71; H, 4.31/4.09; N, 7.19/7.06. Mp. (196.0–198.0) °C. ¹H NMR (CD₂Cl₂, ppm): 27.47 (6H, *w*_{1/2} = 350 Hz). IR (cm⁻¹): 3556 (vw), 3141 (vw), 3054 (vw), 1607 (vw), 1588 (w), 1495 (m), 1436 (m), 1409 (m), 1283 (s), 1266 (sh), 1182 (m), 1113 (s), 1039 (m), 999 (m), 874 (w), 815 (m), 758 (m), 722 (s), 689 (s), 597 (m), 548 (s), 533 (s), 496 (s), 461 (vw), 450 (vw). UV–vis (CH₂Cl₂, cm⁻¹): 14815, 19417, 26316, 33445, 36364, 37175.

(Bu₄N)[Cu₃(μ₃-OH)(μ-pz)₃(NCS)₃] (**8**). Cu(ClO₄)₂·6H₂O (234.8 mg, 0.62 mmol), pzH (41.5 mg, 0.58 mmol), NaOH (33.5 mg, 0.84 mmol), and Bu₄NNCS (187.9 mg, 0.63 mmol) were added to 30 mL of H₂O. The mixture was stirred 1 h, and 20 mL of CH₂Cl₂ were added to form a non aqueous layer. After 1.5 h the organic phase was separated using a separation funnel. Suitable crystals for X-ray diffraction were obtained by Et₂O vapor diffusion to a CH₂Cl₂ solution. Yield: 100.3 mg (62.8% yield) of blue crystals obtained by slow Et₂O vapor diffusion into a CH₂Cl₂ solution. Anal. Calcd/Found: C, 40.74/40.70; H, 5.62/5.34; N, 16.97/17.01. Mp. (141.7–142.2) °C. IR (cm⁻¹): 2961 (w), 2873 (w), 2082 (s), 1478 (w), 1429 (w), 1377 (m), 1279 (w), 1178 (m), 1063 (s), 880 (m), 745 (s), 623 (s), 471 (m), 436 (m). ¹H NMR (CD₃CN, ppm): 40.50 (3H, *w*_{1/2} = 40 Hz); 34.52 (6H, *w*_{1/2} = 70 Hz). UV–vis (CH₃CN, cm⁻¹): 16790, 27460, 32430. **Warning!** Perchlorate salts are explosive.

$[\text{Cu}_3(\mu_3\text{-OH})(\mu\text{-pz})_3(\text{py})_3](\text{CF}_3\text{SO}_3)_2$ (**9**). $\text{Cu}(\text{CF}_3\text{SO}_3)_2$ (0.2277 g, 0.62 mmol), pzH (0.0403 g, 0.58 mmol), NaOH (0.0407 g, 1.02 mmol), and pyridine (53 μL , 0.60 mmol) were stirred in 10 mL of acetone for 24 h at room temperature. The reaction mixture was filtered, and the solvent was reduced to 2 mL under reduced pressure. Yield: 146.6 mg (75.6%) of blue crystals suitable for X-ray diffraction obtained by slow Et_2O vapor diffusion into an acetone solution. Crystals were also obtained by Et_2O diffusion into a THF (or CH_2Cl_2) solution, or by MeOH evaporation. Anal. Calcd/Found: C, 33.07/33.23; H, 2.67/2.77; N, 13.35/13.47. Mp. (219.7–219.9) °C. ^1H NMR (CD_2Cl_2 , ppm): 61.37 (6H, $w_{1/2}$ = 97 Hz); 40.33 (3H, $w_{1/2}$ = 68 Hz); 32.34 (6H, $w_{1/2}$ = 84 Hz); 26.60 (6H, $w_{1/2}$ = 42 Hz); 11.22 (3H, $w_{1/2}$ = 19 Hz); 2.19 ($w_{1/2}$ = 18 Hz). IR (cm^{-1}) 1608 (w), 1491 (w), 1451 (m), 1383 (w), 1250 (s), 1215 (s), 1173 (s), 1070 (s), 1028 (s), 1018 (s), 753 (s), 699 (s), 633 (s), 573 (m), 515 (s), 486 (m) 436 (m). UV–vis (CH_2Cl_2 , cm^{-1}): 17889, 31447.

Results and Discussion

Complexes **4–7** were prepared in similar ways as **1** by either displacement of capping chlorides of $(\text{PPN})_3[\text{Cu}_3(\mu_3\text{-Cl})_2(\mu\text{-R-pz})_3\text{Cl}_3]\text{Cl}$ or from a reaction mixture containing Cu^{2+} , 4-R-pzH and base. Interestingly, by self-assembly the yield was significantly lower for complexes of 4-substituted pyrazolates as the products crystallized in a mixture also containing green and blue crystals identified as $(\text{PPN})_3\text{-}[\text{Cu}_3(\mu_3\text{-Cl})_2(\mu\text{-4-R-pz})_3\text{Cl}_3]\text{Cl}\cdot 3\text{H}_2\text{O}$ and $(\text{PPN})_2[\text{Cu}_3(\mu_3\text{-Cl})(\mu_3\text{-OH})(\mu\text{-4-R-pz})_3\text{Cl}_3]$, respectively. This mixture was separated under the microscope, and violet crystals of the desired $\mu_3\text{-O}$ product were manually isolated and recrystallized from $\text{CH}_2\text{Cl}_2/\text{Et}_2\text{O}$. To isolate **4–7** it is also necessary to add one extra equivalent of PPNCl , as a free Cl-ion co-crystallizes with the complex dianion. Two observations were made while working on the syntheses of **4–7**: First, $\mu_3\text{-O}$ complexes are only isolable from CH_2Cl_2 solutions. Second, PPN^+ counterions are essential to isolate these $\mu_3\text{-O}$ species. There was no crystal growth when Bu_4N^+ was used as counter-cation, and only few crystals were isolated as Ph_4P^+ salts. The latter observations are specifically for $\mu_3\text{-O}$ complexes, while there are $\mu_3\text{-Cl}$ complexes with Cl, Me, and Br substituted pyrazolates and Bu_4N^+ counterions.¹⁶ Only 4-substituted pyrazolates were pursued in this study, since triangular Cu^{II} complexes of 3,5- $\text{R}_2\text{-pz}$ are sterically hindered and none is known to date.¹⁶ Besides **1**, there is only one other trinuclear pyrazolate complex with a $\mu_3\text{-O}$ ligand, also supported by $\mu\text{-pz}$ ligands.²¹ Interestingly, triangular copper-pyrazolate complexes are most frequently synthesized with $\mu_3\text{-OH}$ ligands at the capping position.^{11a,16,22}

Most of the structures involving $\mu_3\text{-OH}$ trinuclear complexes contain a mixed set of three terminal ligands, X, X', and X'', (e.g., $[\text{Cu}_3(\mu_3\text{-OH})(\mu\text{-pz})_3\text{XX}'\text{X}'']$). Mixed-valence complexes with unsymmetrical coordination typically favor charge localization. Symmetrical substitution, $\text{X} = \text{X}' = \text{X}''$, which might favor valence delocalization has only been

reported for Cl,^{11a,23} Br,^{11b} CF_3CO_2 ,⁹ NCO ,¹⁶ CH_3CO_2 ,^{16,22d} and pzH .^{22c} Two new such complexes with $\text{X} = \text{NCS}$ (**8**) and $\text{X} = \text{py}$ (**9**) are reported here.

The original synthetic strategy toward the introduction of new terminal ligands was based on the exchange of the halide ligands in readily available complexes, such as $(\text{Bu}_4\text{N})_2[\text{Cu}_3(\mu_3\text{-Cl})_2(\mu\text{-pz})_3\text{Cl}_3]$, $(\text{PPN})_2[\text{Cu}_3(\mu_3\text{-O})(\mu\text{-pz})_3\text{Cl}_3]$, $(\text{Bu}_4\text{N})[\text{Cu}_3(\mu_3\text{-OH})(\mu\text{-pz})_3\text{Cl}_3]$, and $(\text{Bu}_4\text{N})_2[\text{Cu}_3(\mu_3\text{-Br})_2(\mu\text{-4-Br-pz})_3\text{Br}_3]$ by metathesis.^{11,23} However, when sodium or potassium salts were used in such reactions, the $[\text{Cu-pz}]_3$ metallacycle was opened with concomitant rearrangement forming structures of higher nuclearities.^{16,24} Subsequently, nonhalide copper sources were employed as starting materials.

Accordingly, **8** was prepared by the addition of pyrazole and NaOH to a solution of $\text{Cu}(\text{ClO}_4)_2$ in water. The addition of Bu_4NNCS formed a green oily phase, which was extracted with CH_2Cl_2 , concentrated, and recrystallized by Et_2O vapor diffusion into the CH_2Cl_2 solution. The infrared spectrum of **8** showed a strong band at 2083 cm^{-1} , characteristic of N-coordinated NCS ligands.²⁵

The ^1H NMR spectrum of **8** showed paramagnetically shifted resonances at 40.5 and 34.5 ppm. The presence of only two resonances, one for the protons at the $\text{H}^3/\text{H}^5\text{-pz}$ positions and one for the proton at the $\text{H}^4\text{-pz}$ position, showed the magnetic equivalence of the pyrazolate rings in solution.

Complex **9** was isolated as blue crystals by the addition of a stoichiometric amount of pyridine to a solution of $\text{Cu}(\text{CF}_3\text{SO}_3)_2$, pzH , and NaOH in acetone, CH_2Cl_2 , THF or MeOH. The ^1H NMR spectrum showed the presence of a single species in solution, evident by the five paramagnetically shifted resonances at 61.4, 40.3 (assigned to $\text{H}^1/\text{H}^5\text{-py}$ and $\text{H}^4\text{-pz}$ positions), 32.3, 26.6, and 11.2 ppm (assigned to $\text{H}^3/\text{H}^5\text{-pz}$, $\text{H}^2/\text{H}^4\text{-}$, and $\text{H}^3\text{-py}$ positions).

All attempts of isolating crystalline $\mu_3\text{-O}$ complexes by deprotonation of the $\mu_3\text{-OH}$ group of **8–10** with NaOH or Et_3N were unsuccessful, although UV–vis spectroscopic monitoring of the reactions shows that deprotonation occurs in solution.

X-ray Structures. All complexes described here consist of a nine-membered $[\text{Cu-N-N}]_3$ metallacycle where the Cu-

- (22) (a) Hulsbergen, F. B.; ten Hoedt, R. W. M.; Verschoor, G. C.; Reedijk, J.; Spek, A. L. *J. Chem. Soc., Dalton Trans.* **1983**, 539. (b) Angaroni, M.; Ardizzoia, G. A.; Beringhelli, T.; La Monica, G.; Gatteschi, D.; Masciocchi, N.; Moret, M. *J. Chem. Soc., Dalton Trans.* **1990**, 3305. (c) Sakai, K.; Yamada, Y.; Tsubomura, T.; Yabuki, M.; Yamaguchi, M. *Inorg. Chem.* **1996**, *35*, 542. (d) Casarin, M.; Corvaja, C.; di Nicola, C.; Falcomer, D.; Franco, L.; Monari, M.; Pandolfo, L.; Pettinari, C.; Piccinelli, F.; Tagliatesta, P. *Inorg. Chem.* **2004**, *43*, 5865. (e) Casarin, M.; Corvaja, C.; Di Nicola, C.; Falcomer, D.; Franco, L.; Monari, M.; Pandolfo, L.; Pettinari, C.; Piccinelli, F. *Inorg. Chem.* **2005**, *44*, 6265. (f) Zhou, J.-H.; Liu, Z.; Li, Y.-Z.; Song, Y.; Chen, X.-T.; You, X.-Z. *J. Coord. Chem.* **2006**, *59*, 147. (g) Casarin, M.; Cingolani, A.; Di Nicola, C.; Falcomer, D.; Monari, M.; Pandolfo, L.; Pettinari, C. *Cryst. Growth Des.* **2007**, *7*, 676. (h) Di Nicola, C.; Karabach, Y. Y.; Kirillov, A. M.; Monari, M.; Pandolfo, L.; Pettinari, C.; Pombeiro, A. J. L. *Inorg. Chem.* **2007**, *46*, 221.
- (23) Mezei, G.; Raptis, R. G. *Inorg. Chim. Acta* **2004**, *357*, 3279.
- (24) Mezei, G.; Baran, P.; Raptis, R. G. *Angew. Chem., Int. Ed.* **2004**, *43*, 574.
- (25) Nakamoto, K., *Infrared and Raman Spectra of Inorganic and Coordination Compounds. Part B: Applications in Coordination, Organometallic, and Bioinorganic Chemistry*. 5th ed.; John Wiley & Sons: Canada, 1997; p 270.

(21) Shen, W.-Z.; Peng Cheng, L. Y.; Yan, S.-P.; Liao, D.-Z.; Jiang, Z.-H. *Inorg. Chem. Commun.* **2004**, *7*, 819.

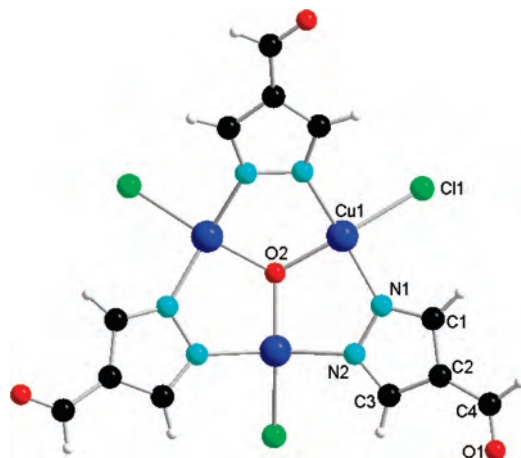


Figure 1. Ball-and-stick diagram of the crystal structure of **6** viewed perpendicular to the 3-fold axis and showing the atom labeling scheme.

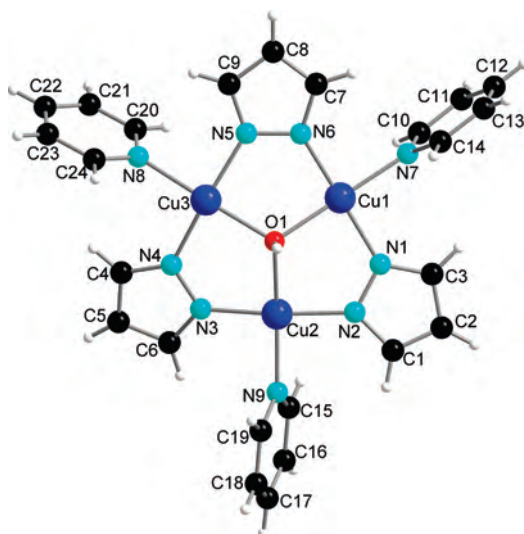


Figure 2. Ball-and-stick diagram of the crystal structure of **9** showing the atom labeling scheme.

atoms are held together by pyrazolate bridges. Complexes **4–7** accommodate an almost planar $\text{Cu}_3(\mu_3\text{-O})$ core (Figure 1), but a pyramidal $\text{Cu}_3(\mu_3\text{-OH})$ moiety forms the core of complexes **8** and **9** (Figure 2). There is no significant variation of the Cu–N, Cu–O, Cu–OH, or $\text{Cu}\cdots\text{Cu}$ distances within complexes **4–9**.

While **4–7** have similar structures to **1**, the presence of halogen-substituents on pyrazole induces significant changes on their solid-state structures. For each of the three complexes, there is a 3-fold symmetry axis running perpendicular to the $[\text{Cu}-\text{N}-\text{N}]_3$ metallacycle, through the oxygen-atom. The Cu–O bond lengths range from 1.889(1) to 1.903(1) Å, while the Cu–O–Cu angles are between 118.6–119.9° for all four complexes. $\text{Cu}\cdots\text{Cu}$ intramolecular distances are within the 3.270–3.275 range. Although $\text{Cu}\cdots\text{Cu}$ and Cu–O distances are similar, the oxygen atom in **4–7** is 0.057–0.223 Å above the Cu_3 -plane, while in **1** it is right in the plane of the three Cu-atoms.^{11a}

Another difference is the orientation of the pyrazole rings relative to the Cu_3 -plane: all three pyrazoles are bent toward the same side of the Cu_3 -plane, opposite to the $\mu_3\text{-O}$ atom; the latter has a water molecule in hydrogen bonding distance

Table 2. Selected Bond Lengths (Å) and Angles (deg) for **6**

Cu(1)–O(2)	1.8971(3)	N(1)–Cu(1)–Cl(1)	92.1(1)
Cu(1)–N(1)	1.950(3)	N(2)–Cu(1)–Cl(1)	93.6(1)
Cu(1)–N(2)	1.954(3)	Cu(1)–O(2)–Cu(1)#1	119.13(6)
Cu(1)–Cl(1)	2.282(1)	Cu(1)–O(2)–Cu(1)#2	119.13(6)
O(2)–Cu(1)#1	1.8971(8)	Cu(1)#1–O(2)–Cu(1)#2	119.13(6)
O(2)–Cu(1)#2	1.8971(8)	C(1)–N(1)–Cu(1)	132.0(3)
O(2)–Cu(1)–N(1)	90.9(1)	N(2)#1–N(1)–Cu(1)	119.9(2)
O(2)–Cu(1)–N(2)	91.2(1)	C(3)#2–N(2)–Cu(1)	132.1(3)
N(1)–Cu(1)–N(2)	157.0(1)	N(1)#2–N(2)–Cu(1)	118.7(2)
O(2)–Cu(1)–Cl(1)	160.0(2)		

($\text{O}\cdots\text{O}$ of 2.359–2.806 Å) along the C_3 -axis. Another feature of these structures is that the three PPN-counteranions, disposed around the C_3 -axis, form a cage that hosts a chloride ion. Complexes **4–6** are isostructural; however, there is no water molecule in the structure of **7**. Important bond lengths and angles for **6** are listed in Table 2.

Complexes **8–9** contain $\mu_3\text{-OH}$ ligands bridging unsymmetrically the three copper atoms. In **8**, three terminal NCS ligands are on the opposite side of their trans- $\mu_3\text{-OH}$ pyramidal group. Cu–NCS and Cu–O bond lengths span the ranges of 1.924(7)–1.957(8) Å and 1.980(6)–2.047(6) Å, respectively. This arrangement holds the copper atoms at distances spanning the range 3.324(4)–3.406(5) Å. All copper atoms are in square-planar N_3O -coordination environments.

The crystal structure of **9** (Figure 2) consists of three terminal py ligands trans to the $\mu_3\text{-OH}$ group with their planes approximately perpendicular to the Cu_3 -plane. For **9**, Cu–N(py), Cu–O bond lengths, and $\text{Cu}\cdots\text{Cu}$ intramolecular distances are within 2.017(6)–2.045(6) Å, 1.999(4)–2.001(4) Å, and 3.320(2)–3.403(4) Å, respectively. One copper atom is in the octahedral N_3O_3 -coordination environment when the long interactions with two triflate anions at 2.681(4)–2.851(9) Å are considered. The two remaining copper atoms are in the square-pyramidal coordination environments by a weak interaction with one acetone and one triflate anion at 2.404(7) Å and 2.456(6) Å, respectively. Important bond lengths and angles for **9** are listed in Table 3.

Electrochemistry. The electrochemical studies of **1** by cyclic voltammetry showed a reversible one-electron oxidation centered at -0.013 V (vs. Fc/Fc^+).⁹ Under the same experimental conditions the corresponding processes to that of **1** were observed for **4–7** (Table 4). However, the redox potentials for **4–7** are influenced by the electron donating ability of the pz ligands, tuned by the 4-R groups. Therefore, the redox potentials are shifted proportionally to the electron-withdrawing capacity of their R-groups in the order $\text{NO}_2 > \text{CHO} > \text{Cl} \sim \text{Br} > \text{H}$. The trend is also consistent with the acidity of 4-R-pyrazoles.²⁶ Moreover, a plot of redox potential as a function of the substituents' Hammett parameter (σ) showed a correlation of 0.989. The correlation between redox potentials and the Hammett parameter has been observed for other series of substituted ligand systems.²⁷ Figure 3 shows the cyclic voltammogram of **1**, **4**, and **6** in the potential range -0.400 to $+0.600$ V (vs. Fc/Fc^+). No

(26) Catalan, J.; Abboud, J. L. M.; Elguero, J. *Adv. Heterocycl. Chem.* **1987**, *41*, 187.

(27) (a) Masui, H.; Lever, A. B. P. *Inorg. Chem.* **1993**, *32*, 2199. (b) Hansch, C.; Leo, A.; Taft, R. W. *Chem. Rev.* **1991**, *91*, 165.

Table 3. Selected Bond Lengths (Å) and Angles (deg) for **9**

Cu(1)–N(6)	1.944(5)	N(6)–Cu(1)–O(1)	88.7(2)	N(3)–Cu(2)–O(1)	89.6(2)	C(6)–N(3)–Cu(2)	129.2(6)
Cu(1)–N(1)	1.951(6)	N(1)–Cu(1)–O(1)	89.4(2)	N(2)–Cu(2)–N(9)	92.1(2)	N(4)–N(3)–Cu(2)	122.2(4)
Cu(1)–O(1)	1.999(4)	N(6)–Cu(1)–N(7)	90.7(2)	N(3)–Cu(2)–N(9)	90.9(2)	C(1)–N(2)–Cu(2)	132.5(5)
Cu(1)–N(7)	2.030(5)	N(1)–Cu(1)–N(7)	90.9(2)	O(1)–Cu(2)–N(9)	169.8(2)	N(1)–N(2)–Cu(2)	119.2(4)
Cu(3)–N(4)	1.955(6)	O(1)–Cu(1)–N(7)	177.1(2)	Cu(1)–O(1)–Cu(2)	112.28(19)	C(3)–N(1)–Cu(1)	132.3(5)
Cu(3)–N(5)	1.963(5)	N(4)–Cu(3)–N(5)	167.2(3)	Cu(1)–O(1)–Cu(3)	113.63(19)	N(2)–N(1)–Cu(1)	120.7(4)
Cu(3)–O(1)	2.001(4)	N(4)–Cu(3)–O(1)	89.4(2)	Cu(2)–O(1)–Cu(3)	116.6(2)	C(10)–N(7)–Cu(1)	121.7(5)
Cu(3)–N(8)	2.045(6)	N(5)–Cu(3)–O(1)	88.9(2)	C(7)–N(6)–Cu(1)	133.1(5)	C(14)–N(7)–Cu(1)	120.3(5)
Cu(2)–N(2)	1.940(6)	N(4)–Cu(3)–N(8)	89.8(2)	N(5)–N(6)–Cu(1)	120.2(4)	C(24)–N(8)–Cu(3)	122.0(5)
Cu(2)–N(3)	1.940(6)	N(5)–Cu(3)–N(8)	90.4(2)	C(9)–N(5)–Cu(3)	130.3(5)	C(20)–N(8)–Cu(3)	119.6(5)
Cu(2)–O(1)	2.000(4)	O(1)–Cu(3)–N(8)	173.5(2)	N(6)–N(5)–Cu(3)	120.6(4)	C(15)–N(9)–Cu(2)	121.0(5)
Cu(2)–N(9)	2.017(6)	N(2)–Cu(2)–N(3)	171.2(2)	C(4)–N(4)–Cu(3)	130.6(6)	C(19)–N(9)–Cu(2)	121.8(5)
N(6)–Cu(1)–N(1)	172.8(2)	N(2)–Cu(2)–O(1)	88.9(2)	N(3)–N(4)–Cu(3)	121.1(4)		

Table 4. Cyclic Voltammetric Data for **4–10**

	R	X	E_{pa} (V)	E_{pc} (V)	$E_{1/2}$ (V)
1	H	Cl	−0.023	−0.083	−0.013
4	Br	Cl	+0.173	+0.110	+0.142
5	Cl	Cl	+0.174	+0.112	+0.143
6	CHO	Cl	+0.309	+0.250	+0.280
7	NO ₂	Cl	+0.483	+0.415	+0.449
2	H	CF ₃ CO ₂	+0.160	+0.101	+0.131
8	H	NCS	+0.253		
9	H	Py	+0.436	+0.364	+0.400
10	H	CH ₃ CO ₂	+0.476		

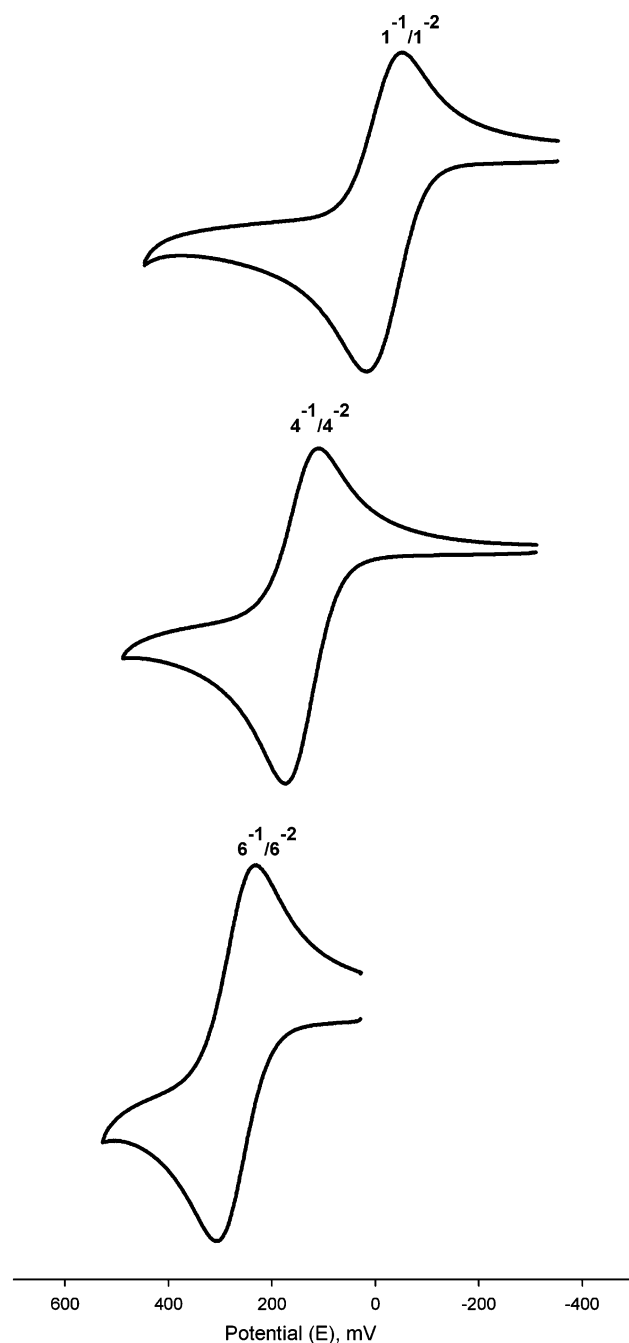
further oxidation was observed for **4–7** up to the solvent oxidation front.

Similarly, the substitution of the terminal chloride by nonhalogen ligands has resulted in shifts of the oxidation potentials. The redox shifts for the different X-ligands are in the order $\text{CH}_3\text{CO}_2 > \text{py} > \text{NCS} > \text{CF}_3\text{CO}_2 > \text{Cl}$. The redox processes are irreversible for the $\text{X} = \text{CH}_3\text{CO}_2$ and NCS species. Addition of anhydrous Et_3N to generate in situ the electrochemically active $\mu_3\text{-O}$ trimer was necessary for **8–10**. The pH-controlled deprotonation of μ_3 -ligands capping the $\text{Cu}_3(\mu\text{-pz})_3$ -frame is well established in this system (Scheme 1).^{11a} Interestingly, there is no redox process observed in the potential window studied for those trimers including hydroxide and chloro bridging ligands under the conditions studied. The results of the electrochemical studies show that complex **1**, with R = H and X = Cl, is the easier oxidized one and therefore the more likely to give a stable one-electron oxidized product.

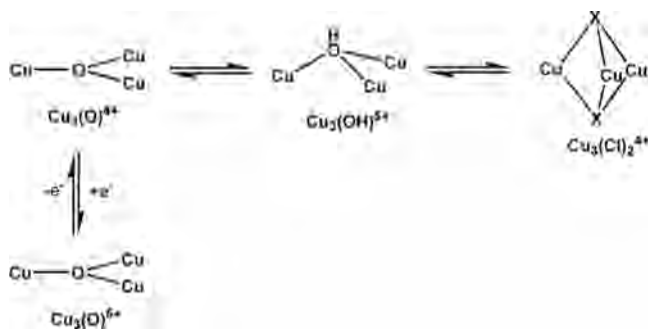
While the $[\text{Cu}_3(\mu_3\text{-O})]^{4+/5+}$ redox processes of **1**, **2**, and **4–7** and **9** are fully reversible on the cyclic voltammetry time scale, bulk chemical oxidation has not yielded stable products under the conditions employed so far. To probe the electronic structure of this elusive mixed-valence species we have attempted the in situ characterization in an OSTLE cell of $[\text{Cu}_3(\mu_3\text{-O})(\mu\text{-pz})_3\text{X}_3]^-$ (**1**[−]) in CH_3CN with 0.25 M Bu_4NPF_6 at 243 K (Figure 4). Even at these conditions, **1**[−] is not perfectly stable resulting in partial blurring of the isosbestic points at 24 100 and 27 000 cm^{-1} . Similar results were obtained in CH_2Cl_2 solvent.

During the one-electron oxidation, the bands at 33 000 and 26 220 cm^{-1} (of **1**^{2−}) shift to 30 280 and 22 200 cm^{-1} (in **1**[−]), respectively. In addition, the mixed-valence complex **1**[−] exhibits a new weak band at 9550 cm^{-1} ($\epsilon = 2600 \text{ cm}^{-1} \text{ M}^{-1}$) attributed to an intervalence charge transfer (IVCT) transition, a characteristic of mixed-valence compounds. The presence of this band in the spectrum of **1**[−] excludes the possibility of a complete valence trapped situation (complete

localization). The detailed analysis of IVCT bands has been the focus of several experimental and theoretical studies, and

**Figure 3.** Cyclic voltammograms for **1** (upper), **4** (middle), and **6** (lower) in CH_2Cl_2 solution.

Scheme 1



recent comprehensive reviews are available.²⁸ In dinuclear systems, the IVCT band energy and half-width depend on the shape of the double-minimum potential well of the electron transfer process and classify a mixed-valent species in the Robin–Day system.²⁹ For $\mathbf{1}^-$, the experimental bandwidth at half-height, $\Delta\nu_{1/2}$, is 1428 cm^{-1} . According to the classical two-state theory, the theoretical bandwidth at half-height ($\Delta\nu_{1/2}^0$) is given by $\Delta\nu_{1/2}^0/\text{cm}^{-1} = [16RT \ln(2) \nu_{\text{max}}]^{1/2}$, where ν_{max} is the IVCT band maximum. In the present case, the observed bandwidth, $\Delta\nu_{1/2}$, is much narrower than the theoretical bandwidth, $\Delta\nu_{1/2}^0 = 4229\text{ cm}^{-1}$, calculated by the above formula. Here the factor $\Gamma = 0.66$ (where $\Gamma = 1 - \Delta\nu_{1/2}/\Delta\nu_{1/2}^0$), characterizing the mixed-valence complex $\mathbf{1}^-$ as a Robin–Day class-III system ($\Gamma > 0.5$): Highly delocalized in the time scale of UV–vis–NIR spectroscopy, in agreement with our earlier theoretical calculations.⁹ For strongly coupled systems, like the present case, the electronic coupling factor H_{ab} is given by $\nu_{\text{max}}/2$.³⁰ Hence, for $\mathbf{1}^-$, $H_{\text{ab}} = 4775\text{ cm}^{-1}$, in close agreement with the value estimated by Belinsky ($\sim 5000\text{ cm}^{-1}$).¹⁰

In contrast to the several dinuclear mixed-valent complexes that have been studied with regard to their electron transfer properties, there is a paucity of studies of larger systems.^{28a} As far as trinuclear systems related to $\mathbf{1}^-$ are concerned,

- (28) (a) D’Alessandro, D. M.; Keene, R. R. *Chem. Rev.* **2006**, *106*, 2270. (b) D’Alessandro, D. M.; Keene, R. R. *Chem. Soc. Rev.* **2006**, *35*, 424. (c) Demadis, K. D.; Hartshorn, C. M.; Meyer, T. J. *Chem. Rev.* **2001**, *101*, 2655. (d) Lunnay, J. P. *Chem. Soc. Rev.* **2001**, *30*, 386.
- (29) (a) Robin, M. B.; Day, P. *Adv. Inorg. Chem. Radiochem.* **1967**, *10*, 247. (b) Allen, C. G.; Hush, N. S. *Prog. Inorg. Chem.* **1967**, *8*, 357. (c) Creutz, C. *Prog. Inorg. Chem.* **1983**, *30*, 1.
- (30) Brunschwig, B.; Creutz, C.; Sutin, N. *Chem. Soc. Rev.* **2002**, *31*, 168.

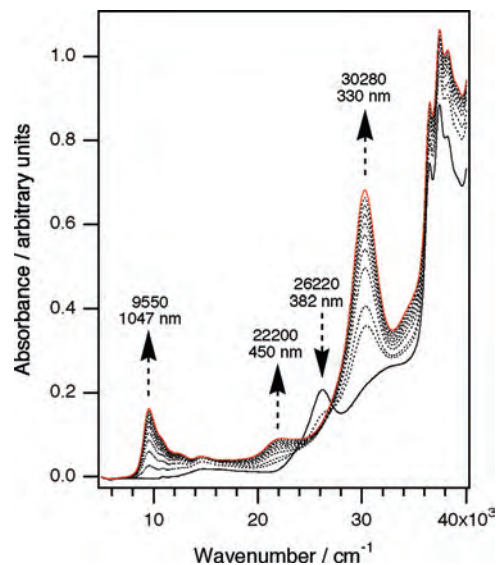


Figure 4. In situ UV–vis–NIR spectra recorded during the oxidation of 1 mM $(\text{PPN})_2[\text{Cu}_3(\mu_3\text{-O})(\mu\text{-pz})_3\text{Cl}_3]$ ($\mathbf{1}$) in CH_3CN with 0.25 M Bu_4NPF_6 at 243 K. The solid black line is the trace of the all- Cu^{II} species ($\mathbf{1}^{2-}$). The red trace is the final spectrum of the oxidized, mixed-valent species ($\mathbf{1}^-$).

IVCT bands have been reported in the cases of $[\text{Fe}_3(\mu_3\text{-O})]^{6+}$ and $[\text{Fe}_2\text{M}(\mu_3\text{-O})]^{n+}$ ($\text{M} = \text{transition metal}$).³¹ Finally, the present results suggest that the postulated triangular, mixed-valent $[\text{Cu}_3(\mu_3\text{-O})]^{5+}$ intermediate^{5b} of pMMO catalytic activity might be straightforwardly characterized by its NIR spectrum, provided it adopts the $^1\text{A}_1$ electronic structure. The importance of detailed spectroscopic analyses of mixed-valent metalloprotein active centers has been recently highlighted.³²

Acknowledgment. M.R.C. and G.M. acknowledge fellowships from NIH-RISE (Grant 2R25GM061151) and NSF-EPSCoR (Grant EPS0223152), respectively.

Supporting Information Available: Crystallographic information files for $\mathbf{4}$ – $\mathbf{9}$. This material is available free of charge via the Internet at <http://pubs.acs.org>.

IC800531Y

- (31) Cannon, R. D.; White, R. P. *Prog. Inorg. Chem.* **1988**, *36*, 195.
 (32) Solomon, E. I.; Xie, X.; Dey, A. *Chem. Soc. Rev.* **2008**, *37*, 623.